Article

Photocatalytic Degradation of Tetracycline by Supramolecular Materials Constructed with Organic Cations and Silver Iodide

Xing-Xing Zhang, Xiao-Jia Wang and Yun-Yin Niu *

Green Catalysis Center, College of Chemistry, Zhengzhou University, Zhengzhou 450001, China
* Correspondence: niuyy@zzu.edu.cn

Abstract: Photocatalytic degradation, as a very significant advanced oxidation technology in the field of environmental purification, has attracted extensive attention in recent years. The design and synthesis of catalysts with high-intensity photocatalytic properties have been the focus of many researchers in recent years. In this contribution, two new supramolecular materials $\{[(L1)\cdot(Ag_4I_7)]CH_3CN\}$ (1), $\{[(L2)\cdot(Ag_4I_7)]CH_3CN\}$ (2) were synthesized by solution volatilization reaction of two cationic templates 1,3,5-Tris(4-aminopyridinylmethyl)-2,4,6-Trimethylphenyl bromide (L1) and 1,3,5-Tris(4-methyl pyridinyl methyl)-2,4,6-trimethylphenyl bromide (L2) with metal salt AgI at room temperature, respectively. The degradation effect of **1** and **2** as catalyst on tetracycline (TC) under visible light irradiation was studied. The results showed that the degradation of TC by **1** was better than that by **2** and both of them had good stability and cyclability. The effects of pH value, catalyst dosage, and anion in water on the photocatalytic performance were also investigated. The adsorption kinetics fit the quasi-first-order model best. After 180 min of irradiation with **1**, the degradation rate of TC can reach 97.91%. In addition, the trapping experiments showed that $\cdot OH$ was the main active substance in the photocatalytic degradation of TC compared with $\cdot O_2^-$ and h^+. Because of its simple synthesis and high removal efficiency, catalyst **1** has potential value for the treatment of wastewater containing organic matter.

Keywords: AgI; supramolecular material; photocatalytic degradation (PDT); tetracycline (TC); catalyst

1. Introduction

In recent years, with the continuous development of the economy and urbanization, chemicals have increasingly been synthesized to meet the growing needs of production and daily life. Unfortunately, various organic pollutants produced in the process of chemical production will cause great harm to water sources [1–3]. Tetracycline (TC) is one of the most widely used antibiotics in poultry and aquaculture [4]. Since most TC antibiotics cannot be metabolized and degraded in organisms, but are excreted as active drugs in feces and urine, they are often detected in the environment [5–8]. In addition, TC is a water-soluble antibiotic, which results in its mobility and long-term persistence in the environment. Therefore, the treatment of tetracycline in wastewater constitutes an important subject of research in environmental protection [9].

A variety of technologies have been proposed by researchers to remove organic pollutants from wastewater [10–16]. Among all technologies, physical adsorption and advanced oxidation processes (AOPs) are considered to be the most promising methods for TC removal because they are more eco-friendly [17–23]. However, adsorption technology can only remove pollutants from water, but not "destroy" pollutants completely. Therefore, the most commonly used method to remove pollutants is AOPs, including photocatalytic oxidation, ultrasonic oxidation, ozonation, wet oxidation, and various combination technologies (Figure 1), which can degrade pollutants by generating highly active, non-selective chemical oxidants (such as H_2O_2, $\cdot OH$, $\cdot O_2^-$, O_3) in situ [24–30]. Among them, photocatalytic oxidation, a method to convert solar energy into chemical energy, is the most sensible

method and has a broad prospect in solving the problem of water pollution [31–33]. An important condition for achieving a good photocatalytic effect is that the photocatalyst has stronger activity; for photocatalytic degradation (PDT), the most important thing is to find an effective, stable, readily available, and excellent catalytic material [34,35].
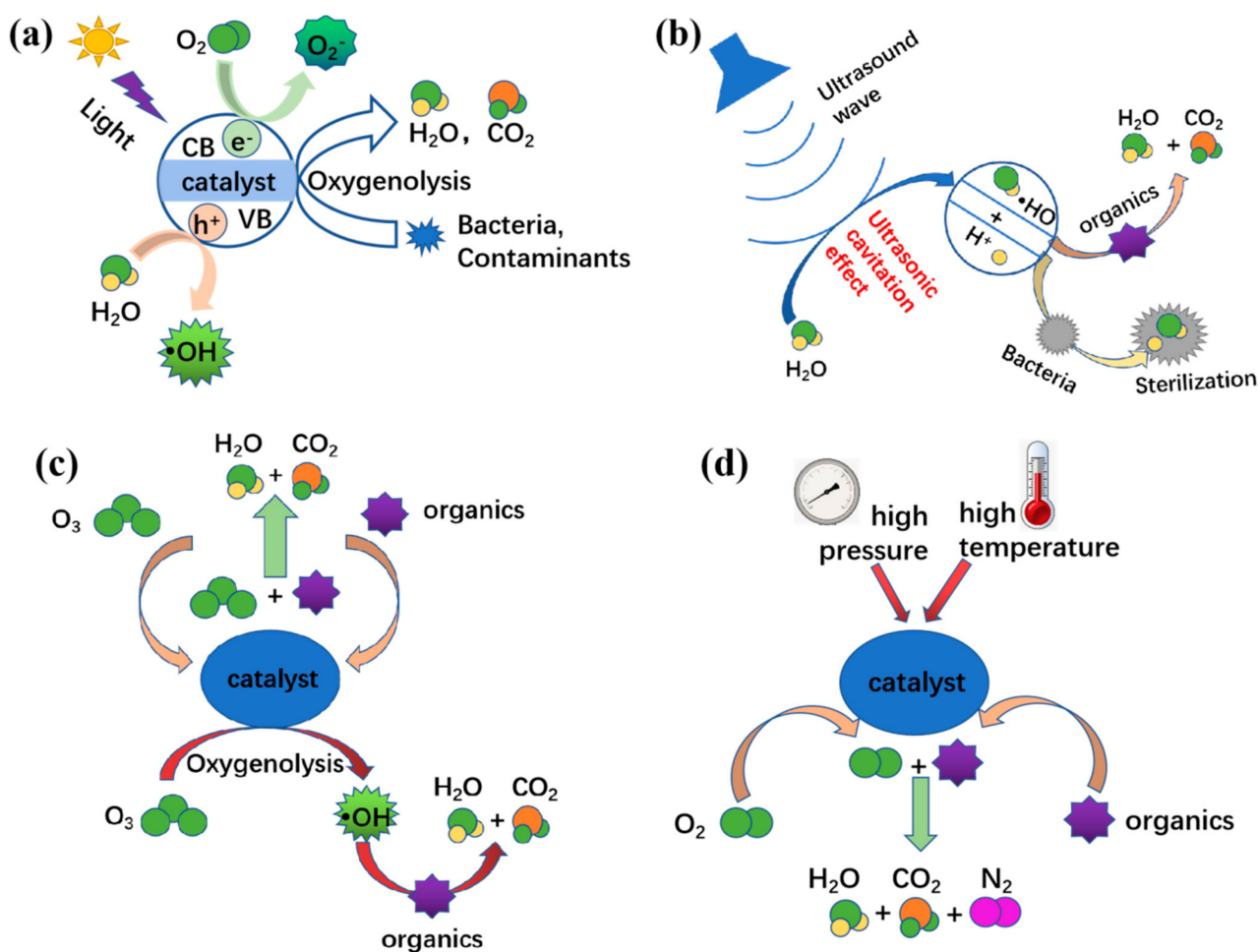

Figure 1. Four commonly used AOPs techniques: (**a**) photocatalytic oxidation technology; (**b**) ultrasonic oxidation technology; (**c**) ozonation technology; (**d**) wet oxidation technology.

Supramolecular chemistry, a complex and ordered combination of molecules with specific functions bonded by non-covalent weak interaction forces, is a sublimation of non-covalent molecular chemistry, known as "chemistry beyond molecular concept". It was first proposed by Jean-Marie Lehn, a French scientist, and was a fringe science composed of multiple disciplines [36,37]. Supramolecules are connected by two or more non-covalent bonding forces between chemical molecules, including hydrogen bonds, Van der Waals forces, electrostatic interactions, host-guest interactions, and π-π stacking [38–42]. Multivalent interactions that rely on noncovalent bonds are an important part of mediating biological processes as well as building complex (super) structures for material applications [43]; only by understanding and controlling non-covalent interactions one can assemble functional nanosystems [44] with a precision similar to nature, and develop highly complex chemical systems and advanced functional materials. Since the advent of supramolecular chemistry, the construction of multi-component supramolecular assemblies, known as supramolecular synthesis [45], has been a hot topic. It not only contains a fundamental understanding of self-assembly and molecular recognition processes related to the origin of life and evolution [46] but also provides support for the design of new materials in the future. Supramolecular compounds have also attracted the attention of

researchers due to their advantages of structurally adjustable and functional diversity. Because the structure of nitrogen-containing heterocyclic ligands is easy to modify, various functional groups can be introduced, and then supramolecular compounds with diverse structures and rich functions can be induced and formed with them as templates, which can be further developed and applied in many fields, such as biomedicine [47,48], optoelectronics [49,50], functional materials [51,52], sensors [53], and so on. Especially in the field of photocatalysis, there have been some reports in recent years about whether supramolecular compounds can be used as photocatalysts. As shown in Table 1, compared with other supramolecular materials, catalysts synthesized by the organic cationic template and AgI have a higher degradation rate for organic pollutants, which offers a promising framework on which to build environmentally friendly materials with high reliability and excellent photocatalytic performance.

Table 1. Research results on the degradation of persistent organic pollutants by supramolecular materials.

Supramolecular Materials and Technologies	Various Research Results on the Degradation of Persistent Organic Pollutants
The supercapacitor and photocatalytic supermolecule materials constructed by 4'4-pyridine and {PMo$_{12}$O$_{40}$}	Zhang et al. reported that the photocatalytic supramolecular material had a good photocatalytic degradation effect on methylene blue (95.8%) and rhodamine B (93.54%) [54].
Photocatalytically Active Supramolecular Organic–Inorganic Magnetic Composites	Sabina et al. prepared composites containing Zn-modified MgAl LDHs and Cu-phthalocyanine as a photosensitizer, which could remove up to 93% of β-lacamide antibiotics from water [55].
AgI/BiPO$_4$ n–n heterojunction photocatalyst	Zhou et al. prepared AgI/BiPO$_4$ n-n heterojunction hybrid by precipitation technology. As a catalyst, the degradation efficiency of this substance for tetracycline hydrochloride (TC) was 95% and methylene blue (MB) was 91%, respectively [56].
Supramolecular photocatalyst of perylene bisimide decorated with α-Fe$_2$O$_3$	Lu et al. prepared α-Fe$_2$O$_3$/PTCDI composite based on supramolecular photocatalyst (PTCDI) modified dinaphthalenediamine (PTCDI) by calcination of ferric nitrate. The degradation rates of phenol pollutants and coking wastewater reached 73% and 66.7%, respectively, by photofenton reaction [57].
Supramolecular Nanopumps with Chiral	Bao et al. prepared ph-responsive supramolecular nanopumps from porous tubules in the left hand to solid fibers in the right hand by self-assembly of aromatic amphiphiles with curved shapes. This superhydrophobic switching aromatic pore is ideal for effective removal and controlled release of organic pollutants from water through pulsating motion. It was found that the removal efficiency of the supramolecular compound was 78% for estradiol and 82% for bisphenol [58].
Two new supramolecular materials {[(L1)·(Ag$_4$I$_7$)]CH$_3$CN} (1), {[(L2)·(Ag$_4$I$_7$)]CH$_3$CN} (2) were synthesized by templatedself-assembly of tetracations L1 and L2 with AgI at room temperature	In this paper the degradation rate of TC by 1 can reach 97.91%.

2. Results and Discussion

2.1. Description of Crystal Structures of {[(L1)·(Ag$_4$I$_7$)]·CH$_3$CN} (1) and {[(L2)·(Ag$_4$I$_7$)]·CH$_3$CN} (2)

The crystal structures of compounds **1** and **2** are similar; both are supramolecular octa-nuclear Ag-I cluster structures belonging to the *P2$_{1/n}$* space group in a monoclinic crystal system. The structural unit diagram of compound **1** is shown in Figure 2a. Metal Ag(I) in compound **1** has a distorted tetrahedral configuration. As shown in Figure 2b, two organic cations are sandwiched around an inorganic anion cluster [Ag$_8$I$_{14}$]$_6{}^-$, which interacts electrically to form a stable 2D supramolecular stacking structure by hydrogen bonding, electrostatic action, and intermolecular force action. The structural unit and packing diagram of catalyst **2** are shown in Figure 2c,d.
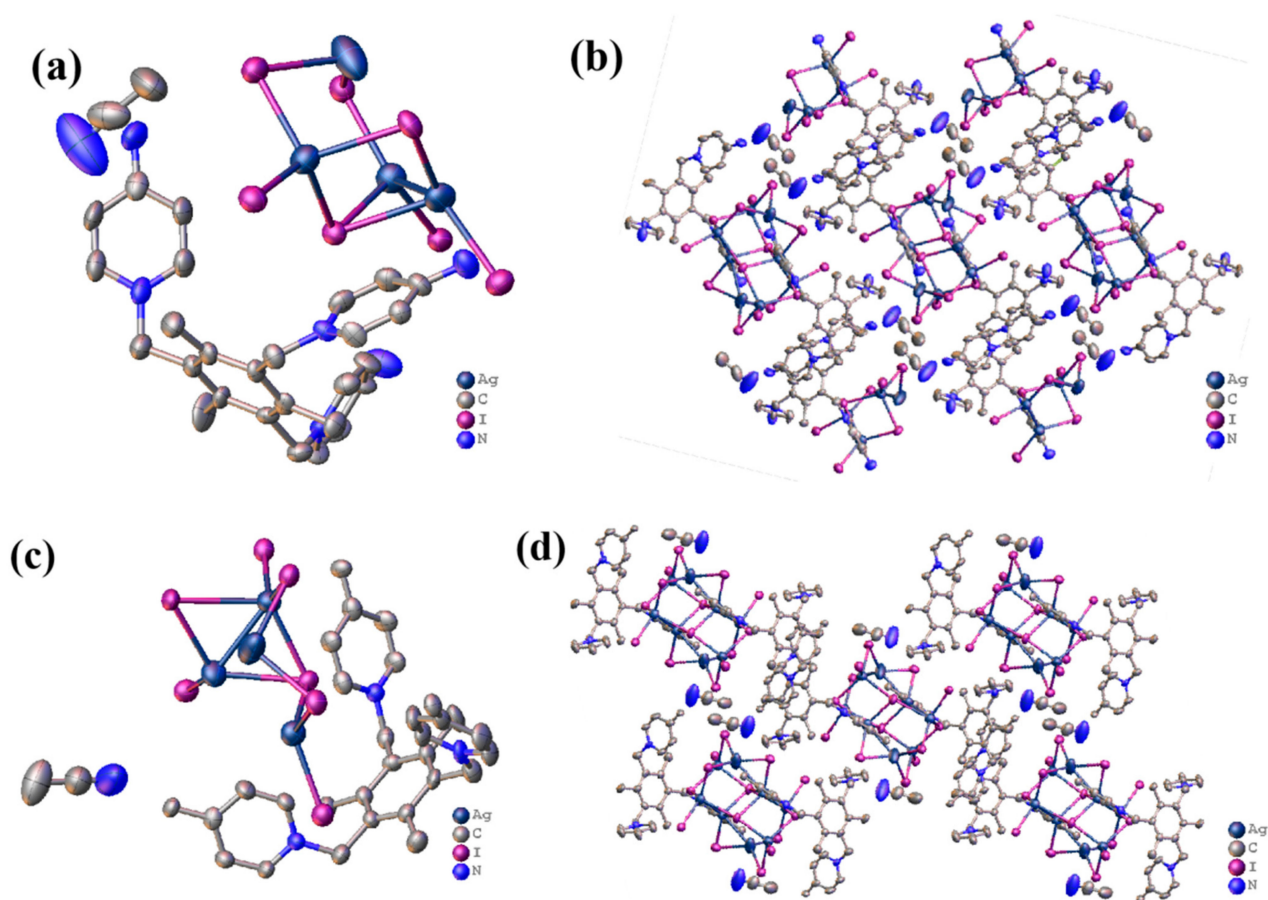
Figure 2. (**a**) The smallest structural unit of catalyst **1**; (**b**) the stacking diagram of catalyst **1**; (**c**) the structural unit of catalyst **2**; (**d**) the stacking diagram of catalyst **2** (with the H atom omitted).

2.2. TG–DTA Analysis

The thermal stability of compounds **1** and **2** was obtained by TG–TDA analysis. As shown in Figure 3a,b, the thermogravimetric degradation trends of compound 1 and compound 2 were similar. They were almost thermally stable between 50 °C and 250 °C; The mass loss between 250 °C and 400 °C may be attributed to the volatile decomposition of solvent molecules and organic cations in the molecule; the mass loss between 400 °C and 800 °C may be caused by the collapse of the inorganic anion skeleton.
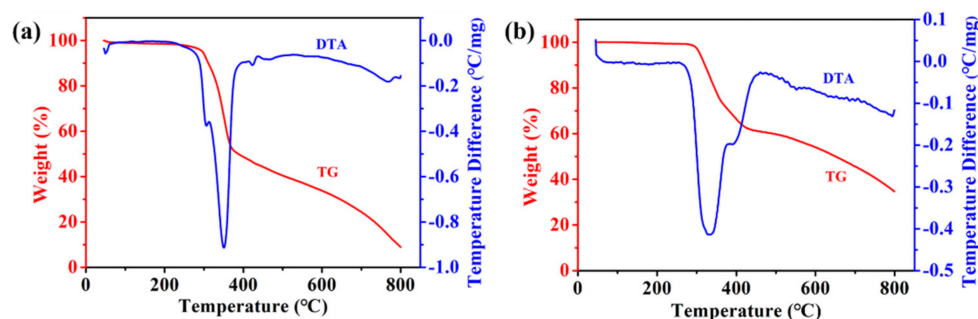

Figure 3. (**a**) TG–DTA curve of compound **1**; and (**b**) TG–DTA curve of compound **2**.

2.3. Semiconductor Properties of Compounds **1** and **2**

The absorption region of light is evaluated by the optical properties of the compounds. To evaluate the semiconductor performance of catalyst **1** and catalyst **2**, the Kubelka-Munk function $F = (1 − R)^2/2R$ [59] was used to calculate their band gap values, as shown

in Figure 4a,b. The band gap values of catalyst **1** and catalyst **2** are 1.62 eV and 2.04 eV, respectively. These results indicate that catalysts **1** and **2** can be used as good semiconductor materials with excellent semiconductor properties and good photocatalytic activity under visible light.
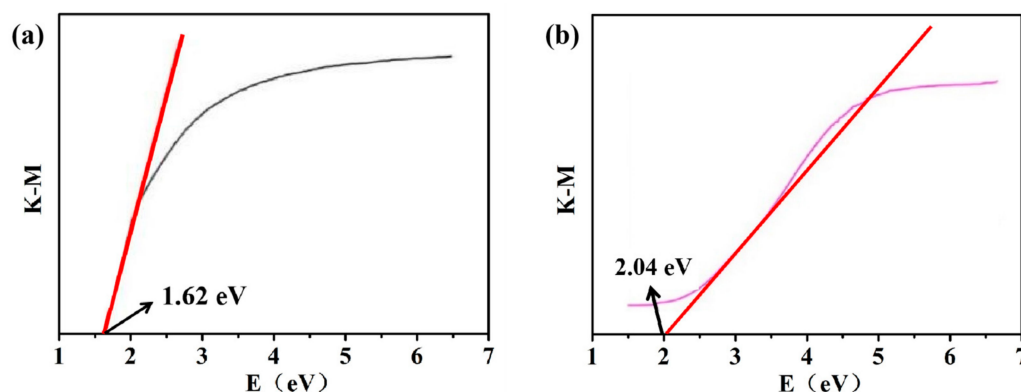

Figure 4. (**a**) Calculation diagram of band gap energy of catalyst **1** (The black line is the absorption curve of catalyst **1**, the red line is the tangent at the approximate linear in the absorption curve, and the intersection of the tangent line and the X-axis is the band gap value); and (**b**) calculation diagram of band gap energy of catalyst **2** (The pink line is the absorption curve of catalyst **2**, the red line is the tangent at the approximate linear in the absorption curve, and the intersection of the tangent line and the X-axis is the band gap value).

2.4. Catalytic Performance of the Degradation of TC with Compounds **1** and **2**

Tetracycline (TC) is an antibiotic widely used in poultry and aquaculture. Because TC cannot be metabolized and degraded in organisms, it is often excreted as raw drugs, which is very harmful to water production. To detect the photocatalytic properties of catalysts **1** and **2**, the organic contaminant TC is selected as the target for photocatalytic degradation. First, 10 mg of catalysts **1** and **2** were added to 20 mL TC solution (20 mg·L^{-1}, pH = 7), and the photocatalytic reaction was carried out in a photoreactor. To eliminate the effect of adsorption on the photocatalytic reaction, additional stirring for 30 min under dark conditions was performed. A 300 W xenon lamp was selected as the visible light source. Under the irradiation of visible light, 3 mL solution was sampled in intervals, separated by centrifugation, and the supernatant was taken. The absorbance of the solution was tested by UV-VIS spectrometer, and then the photocatalytic activity of catalysts **1** and **2** on TC was monitored. As shown in Figure 5a,b, the degradation of TC under visible light is negligible without adding the catalyst. After 180 min of irradiation with catalyst **1**, the degradation rate of TC can reach 97.91%. Furthermore, at 240 min of irradiation, the degradation rate of TC by catalyst **2** was 51.23%, indicating that the degradation efficiency of TC by catalyst **1** was much higher than that by catalyst **2**, which further confirmed the excellent photocatalytic activity of catalyst **1**. Table 2 describes the highest catalytic degradation efficiency of TC in a short time and with different types of catalysts through different treatment systems [60–66]. By comparing the above degradation with the catalyst prepared by us, it can be seen that catalyst 1 has a higher TC removal rate, and its preparation process is safer, easy to operate, and recyclable, and the catalyst is efficiently recovered. Catalyst **1** also had a higher removal rate of TC compared with the above MOFs and hybrid materials. With the increase in reaction time, the removal efficiency of catalysts **1** and **2** reaches equilibrium. In addition, the first-order and second-order kinetics models were used to fit the photocatalytic results, which are shown in Figure 5c,d. It can be seen from the figure that, compared with the second-order kinetics R^2, the first-order kinetics $R^2 > 0.99$, which indicates that first-order kinetics has the best fitting effect. Therefore, the photocatalytic degradation of TC by catalysts **1** and **2** is in line with the photocatalytic process controlled by the first-order kinetics.
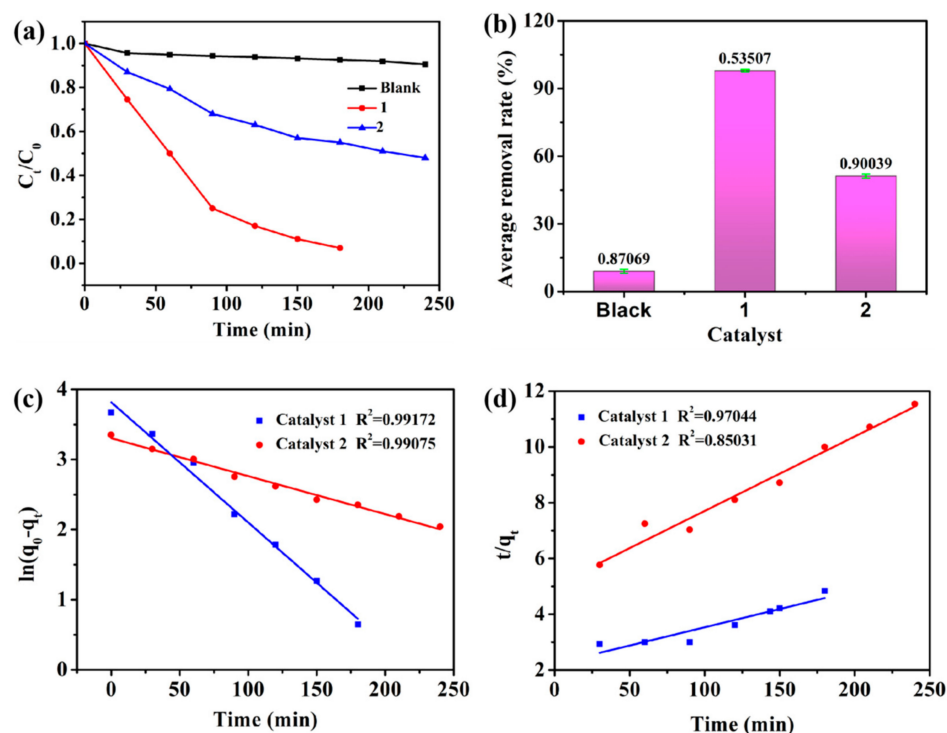
Figure 5. (**a**) The catalytic efficiency of catalysts **1** and **2** on TCs. (**b**) The average removal rate of TC. (**c**) The first-order kinetics of tetracycline degradation by catalysts **1** and **2**. (**d**) The second-order kinetics of tetracycline degradation by catalysts **1** and **2**.

Table 2. Degradation effect of different catalysts on TC.

Treatment System	Catalytic Efficacy of the Catalysts on the TC
Floatable cellulose acetate beads embedded with flower-like zwitterionic binary MOF/PDA	Cao et al. combined SnS_2 nanoparticles (SnSPs), a semiconductor material used for the photodegradation of antibiotics, onto the surface of a zirconia-based organic framework (UiO-66) to obtain a novel photocatalytic material with a degradation rate of 90% for TC [60].
TiO_2/Ag_3PO_4 nanojunctions on carbon fiber cloth	Eman et al. prepared the zwitterionic UiO-66/ZIF-8 binary MOF/polydopamine@cellulose acetate composite (UiO-66/ZIF-8/PDA@CA), the maximum removal rate of TC was 67% [61].
MXene-Based Photocatalysts	Zhang et al. constructed TiO_2/Ag_3PO_4 nanojunction on carbon fiber cloth, and the removal rate of TC from mobile wastewater reached 94.2% [62].
Ag_3PO_4/GO	Wu et al. prepared Ag_3PO_4/GO catalyst by ultrasonic reaction, and after 30 min irradiation, the degradation rate of Ag_3PO_4/5wt%GO to TC was 77.7% [63].
Enhanced sonochemical degradation of tetracycline by sulfate radicals.	Eslami et al. investigated the degradation of antibiotic TC in aqueous solution by silver-activated persulfate ($Na_2S_2O_8$) in the presence of ultrasonic radiation. Under optimal conditions, a TC removal rate of more than 83% was achieved in 120 min [64].
Facet-controlled activation of persulfate by magnetite nanoparticles	Hu et al. synthesized three magnetite nanoparticles (MNPs) with different bare crystal faces by hydrothermal method, and under heterogeneous activation of persulfate (PS), the degradation efficiency of the PS/MNPs {1 1 1} system for TC reached 74.38% within 4 h, which was much higher than that of the PS/MNPs {1 1 0} (19.29%) or PS/MNPs {1 0 0} (33.79%) systems [65].
A yolk-shell Bi@void@SnO_2 photocatalyst	Wu et al. synthesized the yolk-shell Bi@void@SnO_2 photocatalyst by a step-by-step method, and its catalytic degradation efficiency of TC reached 81.81% [66].
Two new supramolecular materials synthesized by templatedself-assembly of tetracations L1 and L2 with AgI	In this paper the degradation rate of TC by 1 can reach 97.91%.

2.5. Effect of pH Solution on TC Degradation

The pH value in the reaction system also plays an important role in the photocatalytic degradation of TC. In this paper, the following experiments were set up: put 20 mL TC solution (20 mg·L^{-1}), and 10 mg catalyst into the photocatalytic reactor, with hydrochloric

acid and sodium hydroxide to adjust the pH value of the solution system to 3, 5, 7, 9, 11 respectively. As shown in Figure 6a,b, the TC degradation efficiencies of catalyst **1** at pH = 3–11 were 53.32%, 89.91%, 97.91%, 63.82%, and 52.65%, respectively. This indicated that the catalytic efficiency increased first and then decreased with the increase in pH value, and the removal efficiency of tetracycline was the highest when the pH value was 7. As shown in Figure 6c,d, the TC degradation efficiencies of catalyst **2** at pH = 3–11 were 37.76%, 41.72%, 67.32%, 70.28%, and 33.65%, respectively. With the increase of pH in the solution, the removal rate of tetracycline also increases at first. When pH = 9, the catalytic effect is the best, and when pH = 11, the degradation rate of photocatalytic tetracycline becomes smaller. The results show that the degradation efficiency at different pH values is related to the difference between the TC charge and the active site of the catalyst. As shown in Figure 6e, most TCs are positively charged (TCH_3^+) at pH < 3; zero charged (TCH_2^0) at neutral, and negatively charged (TCH^- or TC^{2-}) at pH > 7.5. Under acidic conditions, the degradation efficiency of TC by catalysts **1** and **2** at pH = 5 is better than that at pH = 3, mainly because the positively charged TCH_3^+ in the solution will compete with H^+ in the solution for the active site on the catalyst surface. For catalyst **1**, the degradation efficiency at pH = 9 is better than that at pH = 11 under alkaline conditions, mainly because the amino group in catalyst **1** may compete with TCH^- or TC^{2-} for the active site on the surface of the catalyst. When pH is 7, electrostatic force exists, so the removal efficiency of TC reaches the highest. For catalyst **2**, when the pH value changes from 7 to 9, the degradation efficiency of TC continues to improve, because TC becomes negatively charged at this stage and generates electrostatic attraction to catalyst **2**, resulting in an upward trend of degradation efficiency. When pH > 9, the degradation efficiency gradually decreases, possibly because the main form of TC is TC^{2-} exists; it is in contact with the catalyst without electrostatic interaction.
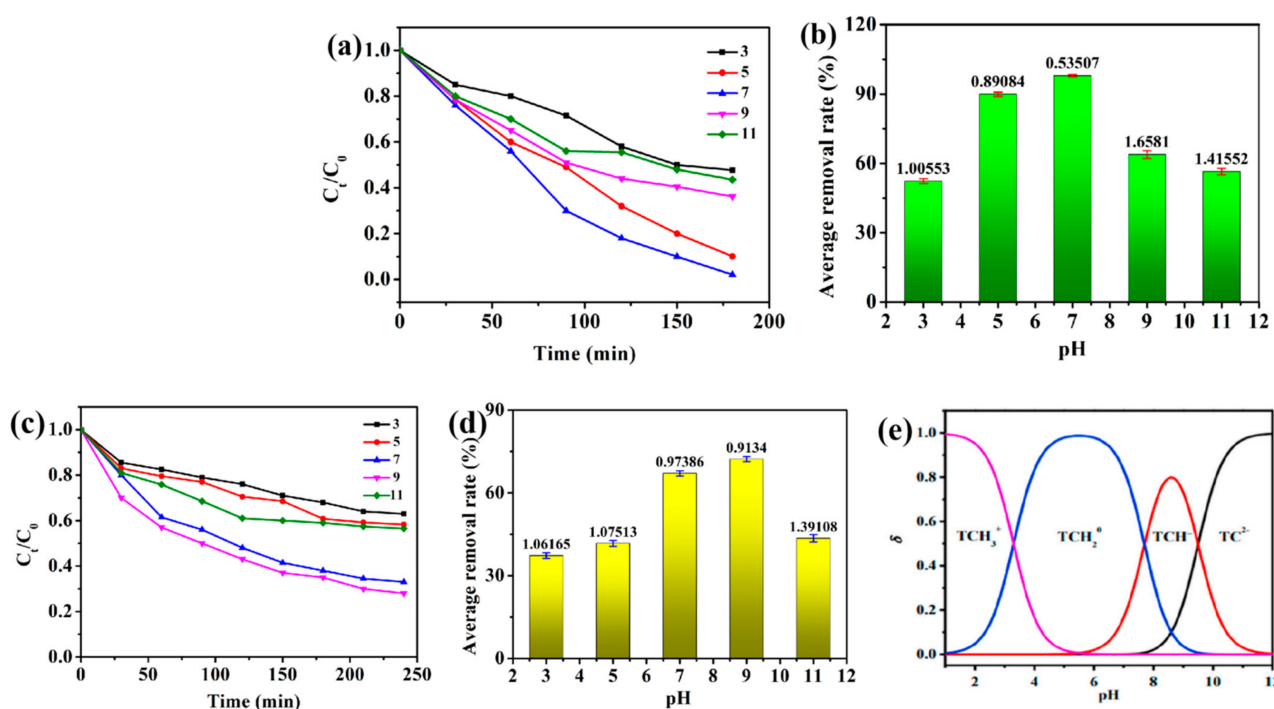

Figure 6. (**a**) Effect of catalyst **1** on TC degradation at different pH conditions. (**b**) Average removal rate of catalyst **1** to TC. (**c**) Effect of catalyst **2** on TC degradation at different pH conditions. (**d**) Average removal rate of catalyst **2** to TC. (**e**) The existence of tetracycline at different pH.

2.6. Effect of the Amount of Catalyst on TC Degradation

In the process of photocatalysis, the dosage of the photocatalyst also plays a vital role. To explore this effect of catalysts **1** and **2** on photocatalytic degradation of TC, 20 mL TC solution with an initial concentration of 20 mg·L^{-1} was taken, and the pH value of the

solution was adjusted to 7 (catalyst **1**) or 9 (catalyst **2**); the catalyst dosage was 5 mg, 10 mg, and 20 mg for photocatalytic reaction. The results are shown in Figure 7a,b. When the amount of catalyst **1** was changed from 5 mg to 20 mg, the degradation rates of TC by it were 74.87%, 97.91%, and 61.27%; the degradation efficiency first increased and then decreased, possibly because with the increase of catalyst acting as adsorbent, the active site provided for photocatalytic reaction increased, and the collision probability between the active site and tetracycline also increased, so the concentration of adsorbent in solution increased. However, the accumulation of excessive catalyst particles will hinder and inhibit the light scattering and transport in the solution, and the organic matter adsorbed on the photocatalyst will reduce the light utilization rate. As shown in Figure 7c,d, the degradation efficiency of TC by catalyst **2** increased from 32.19% to 72.14%, which was due to the increase in the number of active centers with the increase in catalytic dose.
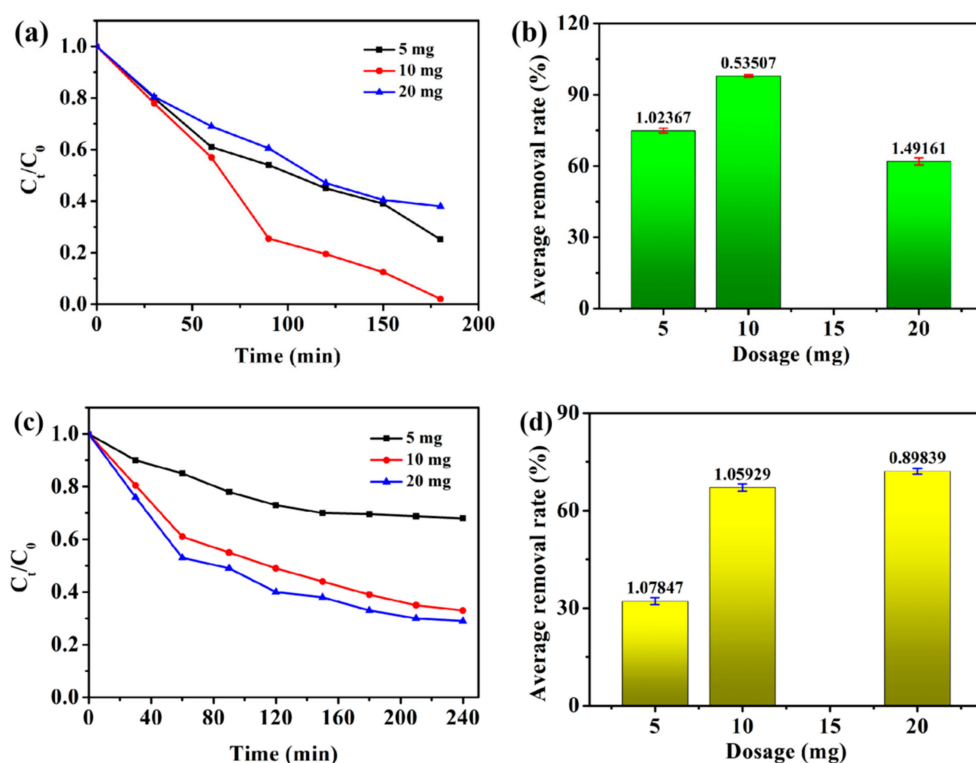

Figure 7. (**a**) Effect of different catalyst **1** dosages on TC degradation. (**b**) Average removal rate of TC degraded by catalyst **1**. (**c**) Effect of different catalyst **2** dosages on TC degradation. (**d**) Average removal rate of TC degraded by catalyst **2**.

2.7. Effects of Anions on Photocatalysis and Catalytic Mechanism

By optimizing the pH value of the TC solution and the number of catalysts, catalyst **1** with higher catalytic efficiency was selected to evaluate the influence of anions and catalytic mechanisms in the photocatalysis process. In this experiment, inorganic anions such as Cl^-, HCO_3^-, NO_3^-, and SO_4^{2-}, which are abundant in antibiotic wastewater in daily life, were selected as experimental subjects. The dosage of the photocatalyst was maintained at 10 mg, the pH of the solution was 7, and the initial concentration of tetracycline solution was 20 mg·L^{-1}. The experimental results are shown in Figure 8a, which clearly shows that the addition of these anions will inhibit the photocatalytic degradation of TC by the catalyst. This is because Cl^-, HCO_3^-, NO_3^- and SO_4^{2-} will combine with ·OH, H^+ or O_2^- to form other free radicals with lower activity, such as NO_3·, SO_4^-·, Cl·, PO_4^{2-}· and HCO_3·/CO_3^-·. To have a deeper understanding of the active free radicals that play a major role in the photocatalytic degradation of TC, three different free radical trapping agents, including isopropanol (IPA, 1 mmol·L^{-1}, ·OH scavenger), ethylenediamine tetraacetic acid disodium

(EDTA–2Na, 1 mmol·L^{-1}, h$^+$ scavenger), and 1,4–p–benzoquinone (PBQ, 1 mmol·L^{-1}, ·O$_2^-$ scavenger) were used to explore the photocatalytic mechanism of the catalyst **1**. The experimental results are shown in Figure 8b. After adding h$^+$ and ·O$_2^-$ capture agent, the photocatalytic degradation efficiency of TC had little change, which indicates that h$^+$ and ·O$_2^-$ hardly contribute to the photocatalytic process, but after adding ·OH capture agent, the photocatalytic efficiency decreased significantly. It is proved that ·OH plays an important role in the photocatalytic degradation of TC. Based on the above experimental results, the following possible photodegradation mechanisms can be proposed. Under the action of visible light, the catalyst composed of two staggered types of semiconductor, L1, and AgI, can induce the excitation of a small negative electron e$^-$ and a small positive hole h$^+$, respectively. After the generation of electron hole pairs, the electrons can transfer from L1 to AgI, and the photogenerated holes transfer in the opposite direction, thus achieving the spatial transfer of photogenerated electron holes, resulting in the photogenerated electrons at the conduction of L1 and the holes at the valence of AgI. The electron holes of L1 and AgI are retained to participate in the REDOX reaction, respectively. The oxygen in the air will produce hydrogen peroxide under the action of the photogenerated electron e$^-$ in the semiconductor L1 and then split into ·OH free radicals. H$_2$O also produces ·OH free radicals under the action of hole h$^+$ in semiconductor AgI. TC molecules can undergo deprotonation, dehydroxylation, demethylation, addition, carboxylation, and benzene ring cleavage under the action of ·OH radical. However, all intermediates eventually mineralize into smaller inorganic molecules, such as NH$_4^+$, NO$_3^-$, H$_2$O, CO$_2$, etc. [67]. The system can not only realize the spatial separation of REDOX sites but also ensure that the photocatalyst can maintain the appropriate valence band position, to maintain a strong REDOX reaction capacity. It was further shown that the added anions interact with the ·OH radical with the highest oxidation potential to form a less active free radical, resulting in reduced pollutant removal efficiency (Figure 8c).
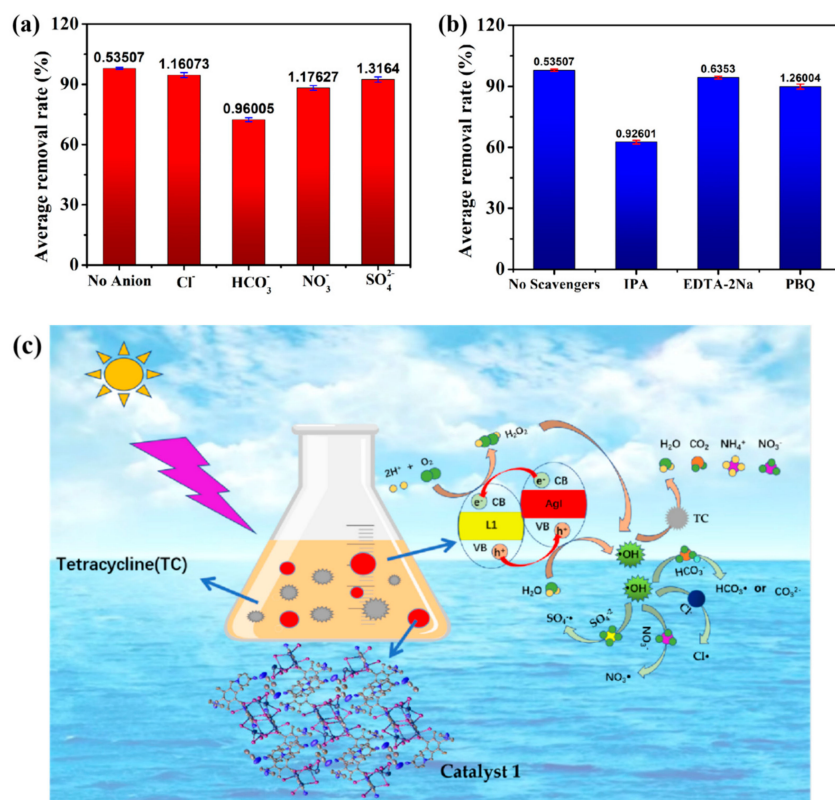

Figure 8. (**a**) Effect of different anions on TC degradation by catalyst **1**. (**b**) Effect of different free radical scavengers on TC degradation by catalyst **1**. (**c**) Photocatalytic degradation mechanism of catalyst **1** under the influence of anions.

2.8. Photocatalyst Recyclability

The reuse and stability of photocatalysts are important criteria for judging the applicable value of the catalyst. The higher the reuse rate, the higher the possibility to put into production and life in the future, which requires the catalyst to maintain excellent catalytic performance in the cycle process. To explore the reusability of catalysts **1** and **2**, cycle experiments were designed to test the photocatalytic efficiency during each cycle. As shown in Figure 9, catalysts **1** and **2** still reached 90.23% and 63.79% in the third round (97.91% and 71.28% in the first round, respectively), indicating that the photocatalytic degradation efficiency of these two catalysts did not decrease significantly. It is proven that catalysts **1** and **2** have easy recovery and good stability.
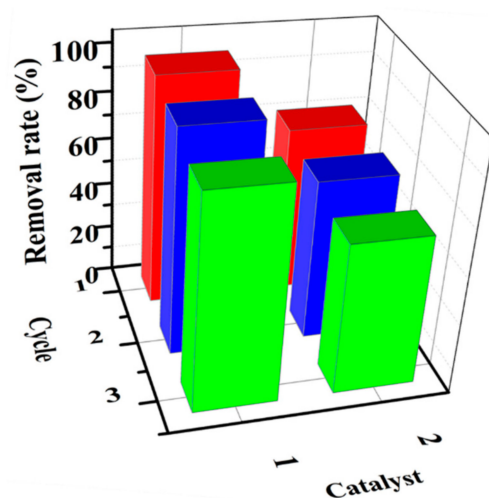

Figure 9. The effect diagram of the TC/catalysts **1** and **2** system for three cycles.

3. Materials and Methods

3.1. Materials

All the reagents of AR grade were used without any further purification. The cationic templates 1,3,5–Tris(4–aminopyridinylmethyl)–2,4,6–trimethylphenyl bromide (L1) [68] and 1,3,5–Tris(4–methylpyridinylmethyl)–2,4,6–trimethylphenyl bromide (L2) [69] were synthesized according to the methods described in the literature (Figure 10).
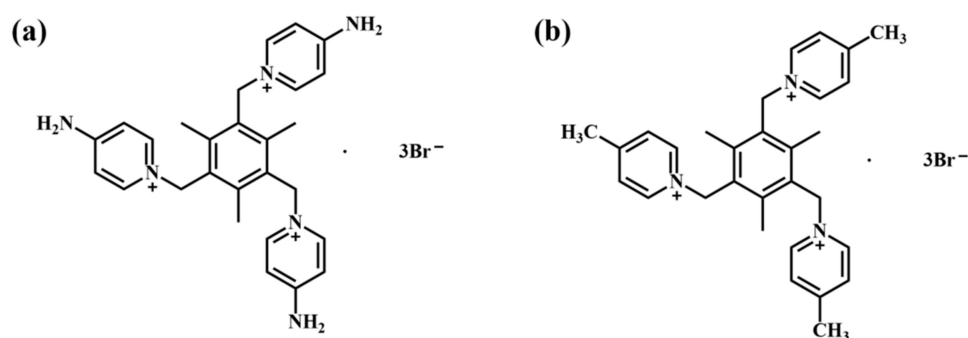

Figure 10. (**a**) The cationic template L1; and (**b**) the cationic template L2.

3.2. Synthesis of Compounds

3.2.1. The Synthesis of {[(L1)·(Ag$_4$I$_7$)]·CH$_3$CN} **1**

L1 (0.0068 g, 0.01 mmol) in MeCN (3 mL) was added to AgI (0.0024 g, 0.01 mmol) in MeCN (2 mL) in the presence of an appropriate amount of KI, and then the mixed solution was stirred for 10 min and filtrated. The filtrate was volatilized at room temperature for 3 days, and colorless transparent columnar crystals were harvested. The yield was 15%. IR

(KBr, cm^{-1}): 3295.49 (s), 3179.36 (s), 2974.37 (s), 2926.54 (s), 1660.81 (s), 1558.41 (m), 1508.76 (s), 1456.24 (m), 1376.24 (s), 1291.79 (m), 1170.65 (s), 049.76 (s), 880.89 (w), 833.86 (s), 521.54 (w), 499.19 (w). Elemental Anal. Calc. For $C_{29}H_{36}N_7Ag_4I_7$ (1802.45): C, 19.32; H, 2.01; N, 5.44%. Found: C, 19.42; H, 2.48; N, 5.56%.

3.2.2. The Synthesis of {[(L2)·(Ag$_4$I$_7$)]·CH$_3$CN} 2

L2 (0.0068 g, 0.01 mmol) in MeCN (3 mL) was added to AgI (0.0024 g, 0.01 mmol) in DMF (3 mL) in the presence of an appropriate amount of KI, and then the mixed solution was stirred for 10 min and filtrated. Finally, the filtrate was volatilized at room temperature for 2 weeks, and colorless transparent crystals were harvested. The yield was 10%. IR (KBr, cm^{-1}): 3440 (s), 2923 (m), 2853 (s), 1635(s), 1463 (w), 1403(w), 1262(w), 936 (s), 801 (s), 516 (w). Elemental Anal. Calc. for $C_{32}H_{39}N_4Ag_4I_7$ (1799): C, 21.35; H, 2.18; N, 3.11. Found: C, 21.38 H,2.23; N, 3.15.

3.3. Methods for Characterizing Compounds

The KBr tablet pressing method and the Bruker TENSOR 27 infrared spectrometer were used to test the infrared spectrum (IR) in the range of 400 to 4000 cm^{-1} (Bruker, Shanghai, China). The NETZSCHTG209 thermogravimetric analyzer (Netzsch, Shanghai, China) was used to record changes in sample mass during a temperature rise from room temperature to 800 °C in a nitrogen atmosphere at a temperature rate of 5 °C·min^{-1}. Elemental analyses (C, H, and N) were performed on a Perkin-Elmer 240 elemental analyzer (PerkinElmer, Shanghai, China). UV-visible spectra were studied with a UV-5500 PC spectrophotometer in the scanning range of 200–800 nm. Using a graphite monochrome Cu-Kα light source (λ = 0.15418 nm) (XRD-6100, Shimadzu, Kyoto, Japan), setting the scan step to 2θ, the angular velocity of 4°·min^{-1}, and scanning range 5–50°, Powder X-ray diffraction (PXRD) data were tested with Philips X-pert X-ray diffraction (PXRD) with an X′Celerator detector. Simulation of the PXRD spectra was carried out by the single-crystal data and diffraction-crystal module of the Mercury (Hg) program. For compounds **1** and **2**, the synthesized PXRD plot is very close to the simulated single crystal diffraction pattern, indicating that the product is pure; their PXRD patterns were shown in Figure 11a,b. The compounds used Mo-Kα rays (λ = 0.71073 Å) for X-ray detection and crystallography data collection at the Bruker SMART CCD X-single crystal diffractometer. The structure was refined with full-matrix least-squares techniques on F^2 using the OLEX2 program package.
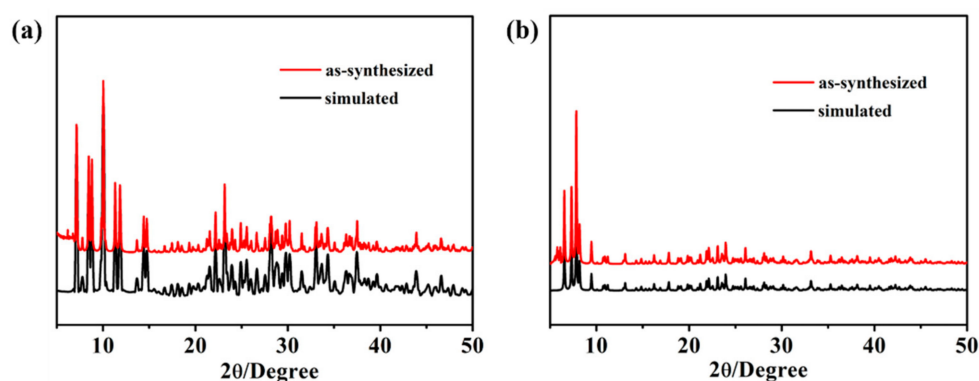

Figure 11. (**a**) PXRD pattern of catalyst **1**; and (**b**) PXRD pattern of catalyst **2**.

4. Conclusions

In this chapter, two supramolecular materials **1** and **2** were synthesized by solution volatilization at room temperature. Through a series of characterizations, it was proved that they had good catalytic potential, and the optimal conditions of photocatalytic degradation of TC were explored. The experimental results showed that for TC solution with the initial concentration of 20 mg·L^{-1}, the degradation rate of TC reached 97.91% after 180 min at pH = 7 with catalyst **1** of 10 mg. When the catalytic dose of catalyst **2** was 20 mg at

pH = 9. The degradation rate of tetracycline reached 71.28% after 240 min of reaction. The photocatalytic degradation effect of catalyst **1** on TC was better than that of catalyst **2**. The inorganic anions in the system (Cl^-, NO_3^-, SO_4^{2-}, and HCO_3^-, etc.) can inhibit the photocatalytic degradation of the TC, because the ionic radicals (such as $Cl\cdot$, $NO_3\cdot$, $SO_4^-\cdot$, and $HCO_3\cdot/CO_3^-\cdot$) with lower activity than $\cdot OH$ or $\cdot O_2^-$ are generated. By adding free radical trapping agents it is shown that the $\cdot OH$ active free radicals play a major role in the photocatalytic reaction process. Through the photocatalytic cycle experiment, it was found that catalysts **1** and **2** still had high photocatalytic efficiency after three cycles, which fully proved the stability and repeatability of catalysts **1** and **2**. This study is helpful to solve the problem of water contamination by antibiotics. In subsequent studies, the detailed HRETM and XPS, together with the PL/RAMAN spectroscopy analysis can be conducted to further to provide information such as the lattice fridge, chemical state and electronic state of the elements, or charge carrier trapping, immigration, and transfer within the systems of catalysts 1 and 2.

Author Contributions: Conceptualization, X.-X.Z., X.-J.W. and Y.-Y.N.; methodology, X.-X.Z., X.-J.W. and Y.-Y.N.; software, X.-X.Z.; validation, X.-X.Z., X.-J.W. and Y.-Y.N.; formal analysis, Y.-Y.N.; investigation, X.-X.Z., X.-J.W. and Y.-Y.N.; resources, X.-J.W.; data curation, X.-X.Z.; writing—original draft preparation, X.-X.Z. and Y.-Y.N.; writing—review and editing, X.-X.Z. and Y.-Y.N.; visualization, X.-X.Z. and Y.-Y.N. All authors have read and agreed to the published version of the manuscript.

Conflicts of Interest: The authors declare no conflict of interest.

References

1. Salipira, K.L.; Mamba, B.B.; Krause, R.W.; Malefetse, T.J.; Durbach, S.H. Carbon nanotubes and cyclodextrin polymers for removing organic pollutants from water. *Environ. Chem. Lett.* **2006**, *5*, 13–17. [CrossRef]
2. Wojtyla, S.; Baran, T. Insight on doped ZnS and its activity towards photocatalytic removing of Cr(VI) from wastewater in the presence of organic pollutants. *Mater. Chem. Phys.* **2018**, *212*, 103–112. [CrossRef]
3. Zhuang, H.M.; Zhang, W.M.; Wang, L.; Zhu, Y.Y.; Xi, Y.Y.; Lin, X.F. Vapor Deposition-Prepared MIL-100(Cr)- and MIL-101(Cr)-Supported Iron Catalysts for Effectively Removing Organic Pollutants from Water. *ACS Omega* **2021**, *63*, 25311–25322. [CrossRef]
4. Liu, J.; Deng, W.J.; Ying, G.G.; Tsang, E.P.K.; Hong, H.C. Occurrence and distribution of antibiotics in surface water. *Ecotoxicology* **2022**, *31*, 1111–1119. [CrossRef]
5. Couch, M.; Agga, G.E.; Kasumba, J.; Parekh, R.R.; Loughrin, J.H.; Conte, E.D. Abundances of Tetracycline Resistance Genes and Tetracycline Antibiotics during Anaerobic Digestion of Swine Waste. *J. Environ. Qual.* **2019**, *48*, 171–178. [CrossRef] [PubMed]
6. Li, P.Y.; Rao, D.M.; Wang, Y.M.; Hu, X.R. Adsorption characteristics of polythiophene for tetracyclines and determination of tetracyclines in fish and chicken manure by solid phase extraction-HPLC method. *Microchem. J.* **2021**, *173*, 106935. [CrossRef]
7. Du, L.F.; Liu, W.K. Occurrence, fate, and ecotoxicity of antibiotics in agro-ecosystems: A review. *Agron. Sustain. Dev.* **2011**, *32*, 309–327. [CrossRef]
8. Kuppusamy, S.; Kakarla, D.; Venkateswarlu, K.; Megharaj, M.; Yoon, Y.E.; Lee, Y.B. Veterinary antibiotics (VAs) contamination as a global agro-ecological issue: A critical view. *Agric. Ecosyst. Environ.* **2018**, *257*, 47–59. [CrossRef]
9. Zhou, Y.; Yang, Q.; Zhang, D.N.; Gan, N.; Li, Q.P.; Cuan, J. Detection and removal of antibiotic tetracycline in water with a highly stable luminescent MOF. *Sens. Actuators B Chem.* **2018**, *262*, 137–143. [CrossRef]
10. Li, J.; Wang, X.X.; Zhao, G.X.; Chen, C.L.; Chai, Z.F.; Alsaedi, A.; Hayat, T.; Wang, X.K. Metal–organic framework-based materials: Superior adsorbents for the capture of toxic and radioactive metal ions. *Chem. Soc. Rev.* **2018**, *47*, 2322–2356. [CrossRef]
11. Zhao, G.X.; Huang, X.B.; Tang, Z.W.; Huang, Q.F.; Niu, F.L.; Wang, X.K. Polymer-based nanocomposites for heavy metal ions removal from aqueous solution: A review. *Polym. Chem.* **2018**, *9*, 3562–3582. [CrossRef]
12. Fu, S.F.; Chen, K.Q.; Zou, H.; Xu, J.X.; Zheng, Y.; Wang, Q.F. Using calcium peroxide (CaO_2) as a mediator to accelerate tetracycline removal and improve methane production during co-digestion of corn straw and chicken manure. *Energy Convers. Manag.* **2018**, *172*, 588–594. [CrossRef]
13. Oturan, N.; Wu, J.; Zhang, H.; Sharma, V.K.; Oturan, M.A. Electrocatalytic destruction of the antibiotic tetracycline in aqueous medium by electrochemical advanced oxidation processes: Effect of electrode materials. *Appl. Catal. B* **2013**, *140*, 92–97. [CrossRef]
14. Yu, L.L.; Cao, W.; Wu, S.C.; Yang, C.; Cheng, J.H. Removal of tetracycline from aqueous solution by MOF/graphite oxide pellets: Preparation, characteristic, adsorption performance and mechanism. *Ecotoxicol. Environ. Saf.* **2018**, *164*, 289–296. [CrossRef]

15. Park, J.-A.; Nam, A.; Kim, J.-H.; Yun, S.-T.; Choi, J.-W.; Lee, S.-H. Blend-electrospun graphene oxide/Poly(vinylidene fluoride) nanofibrous membranes with high flux, tetracycline removal and anti-fouling properties. *Chemosphere* **2018**, *207*, 347–356. [CrossRef] [PubMed]

16. Wang, X.J.; Qiao, X.Y.; Li, Z.Y.; Wei, D.H.; Niu, Y.Y. Influence of 4-cyanopyridinium multicationic isomers on the structure-property relationships of two-dimensional hybrid as photocatalyst for the degradation of organic dyes. *Inorg. Chem. Commun.* **2020**, *119*, 108126. [CrossRef]

17. Li, H.P.; Dou, Z.; Chen, S.Q.; Hu, M.; Li, S.; Sun, H.M.; Jiang, Y.C.; Zhai, Q.G. Design of a Multifunctional Indium–Organic Framework: Fluorescent Sensing of Nitro Compounds, Physical Adsorption, and Photocatalytic Degradation of Organic Dyes. *Inorg. Chem.* **2019**, *58*, 11220–11230. [CrossRef]

18. Deng, S.Q.; Mo, X.J.; Zheng, S.R.; Jin, X.; Gao, Y.; Cai, S.L.; Fan, J.; Zhang, W.G. Hydrolytically Stable Nanotubular Cationic Metal–Organic Framework for Rapid and Efficient Removal of Toxic Oxo-Anions and Dyes from Water. *Inorg. Chem.* **2019**, *58*, 2899–2909. [CrossRef]

19. Ma, H.F.; Liu, Q.Y.; Wang, Y.L.; Yin, S.G. A Water-Stable Anionic Metal–Organic Framework Constructed from Columnar Zinc-Adeninate Units for Highly Selective Light Hydrocarbon Separation and Efficient Separation of Organic Dyes. *Inorg. Chem.* **2017**, *56*, 2919–2925. [CrossRef]

20. Feng, L.Y.; Li, X.Y.; Chen, X.T.; Huang, Y.J.; Peng, K.S.; Huang, Y.X.; Yan, Y.Y.; Chen, Y.G. Pig manure-derived nitrogen-doped mesoporous carbon for adsorption and catalytic oxidation of tetracycline. *Sci. Total Environ.* **2019**, *708*, 135071. [CrossRef] [PubMed]

21. Giammarco, J.; Mochalin, V.N.; Haeckel, J.; Gogotsi, Y. The adsorption of tetracycline and vancomycin onto nanodiamond with controlled release. *J. Colloid Interface Sci.* **2016**, *468*, 253–261. [CrossRef]

22. Wang, D.; Jia, F.; Wang, H.; Chen, F.; Fang, Y.; Dong, W.; Zeng, G.; Li, X.; Yang, Q.; Yuan, X. Simultaneously efficient adsorption and photocatalytic degradation of tetracycline by Fe-based MOFs. *J. Colloid Interface Sci.* **2018**, *519*, 273–284. [CrossRef] [PubMed]

23. Zhang, S.P.; Li, Y.K.; Shi, C.H.; Guo, F.Y.; He, C.Z.; Cao, Z.; Hu, J.; Cui, C.Z.; Liu, H.L. Induced-fit adsorption of diol-based porous organic polymers for tetracycline removal. *Chemosphere* **2018**, *212*, 937–945. [CrossRef]

24. Dewil, R.; Mantzavinos, D.; Poulios, I.; Rodrigo, M.A. New perspectives for Advanced Oxidation Processes. *J. Environ. Manag.* **2017**, *195*, 93–99. [CrossRef]

25. Babu, S.G.; Ashokkumar, M.; Neppolian, B. The Role of Ultrasound on Advanced Oxidation Processes. *Top. Curr. Chem.* **2016**, *374*, 75. [CrossRef] [PubMed]

26. Bavasso, I.; Montanaro, D.; Petrucci, E. Ozone-based electrochemical advanced oxidation processes. *Curr. Opin. Electrochem.* **2022**, *34*, 101017. [CrossRef]

27. Wang, J.L.; Zhuan, R. Degradation of antibiotics by advanced oxidation processes: An overview. *Sci. Total Environ.* **2019**, *701*, 135023. [CrossRef] [PubMed]

28. De Filpo, G.; Pantuso, E.; Mashin, A.I.; Baratta, M.; Nicoletta, F.P. WO_3/Buckypaper Membranes for Advanced Oxidation Processes. *Membranes* **2020**, *45*, 157. [CrossRef]

29. Bethi, B.; Sonawane, S.H.; Bhanvase, B.A.; Gumfekar, S.P. Nanomaterials-based advanced oxidation processes for wastewater treatment: A review. *Chem. Eng. Process.* **2016**, *109*, 178–189. [CrossRef]

30. Dai, Q.Z.; Zhou, M.H.; Lei, L.C.; Zhang, X.W. A novel advanced oxidation process—Wet electro-catalytic oxidation for high concentrated organic wastewater treatment. *Sci. Bull.* **2007**, *52*, 1724–1727. [CrossRef]

31. Wang, X.Y.; Li, S.N.; Chen, P.; Li, F.X.; Hu, X.M.; Hua, T. Photocatalytic and antifouling properties of TiO_2-based photocatalytic membranes. *Mater. Today Chem.* **2021**, *23*, 100650. [CrossRef]

32. Koe, W.S.; Lee, J.W.; Chong, W.C.; Pang, Y.L.; Sim, L.C. An overview of photocatalytic degradation: Photocatalysts, mechanisms, and development of photocatalytic membrane. *Environ. Sci. Pollut. Res.* **2019**, *27*, 2522–2565. [CrossRef] [PubMed]

33. Chang, P.; Wang, Y.H.; Wang, Y.T.; Zhu, Y.Y. Current trends on In_2O_3 based heterojunction photocatalytic systems in photocatalytic application. *Chem. Eng. J.* **2022**, *450*, 137804. [CrossRef]

34. Qiao, X.Y.; Wang, C.H.; Niu, Y.Y. N-Benzyl HMTA induced self-assembly of organic-inorganic hybrid materials for efficient photocatalytic degradation of tetracycline. *J. Hazard. Mater.* **2020**, *391*, 122121. [CrossRef] [PubMed]

35. Wang, X.J.; Qiao, G.Y.; Zhu, G.H.; Li, J.; Guo, X.Y.; Liang, Y.; Niu, Y.Y. Preparation of 2D supramolecular material doping with TiO_2 for degradation of tetracycline. *Environ. Res.* **2021**, *202*, 111689. [CrossRef]

36. Zhou, C.H.; Gan, L.L.; Zhang, Y.Y.; Zhang, F.F.; Wang, G.Z.; Jin, L.; Geng, R.X. Review on supermolecules as chemical drugs. *Sci. China Chem.* **2009**, *52*, 415–458. [CrossRef]

37. Vicens, J.; Vicens, Q. Emergences of supramolecular chemistry: From supramolecular chemistry to supramolecular science. *J. Incl. Phenom. Macrocycl. Chem.* **2011**, *71*, 251–274. [CrossRef]

38. Lu, D.P.; Huang, Q.; Wang, S.D.; Wang, J.Y.; Huang, P.S.; Du, P.W. The Supramolecular Chemistry of Cycloparaphenylenes and Their Analogs. *Front. Chem.* **2019**, *7*, 668. [CrossRef]

39. Leclercq, L.; Douyère, G.; Nardello-Rataj, V. Supramolecular Chemistry and Self-Organization: A Veritable Playground for Catalysis. *Catalysts* **2019**, *9*, 163. [CrossRef]

40. Prins, L.J.; Reinhoudt, D.N.; Timmerman, P. Noncovalent Synthesis Using Hydrogen Bonding. *Angew. Chem. Int. Ed.* **2001**, *40*, 2382–2426. [CrossRef]

41. Adams, H.; Hunter, C.A.; Lawson, K.R.; Perkins, J.; Spey, S.E.; Urch, C.J.; Sanderson, J.M. A supramolecular system for quantifying aromatic stacking interactions. *Chem. Eur. J.* **2002**, *7*, 4863–4877. [CrossRef]

42. Müller-Dethlefs, K.; Hobza, P. Noncovalent interactions: A challenge for experiment and theory. *Chem. Rev.* **2001**, *100*, 143–168. [CrossRef]

43. Badjić, J.D.; Nelson, A.; Cantrill, S.J.; Turnbull, W.B.; Stoddart, J.F. Multivalency and cooperativity in supramolecular chemistry. *Acc. Chem. Res.* **2005**, *38*, 723–732. [CrossRef]

44. Philp, D.; Stoddart, J.F. Self-Assembly in Natural and Unnatural Systems. Angew. *Chem. Int. Ed.* **1996**, *35*, 1154–1196. [CrossRef]

45. Fyfe, M.C.T.; Stoddart, J.F. Synthetic Supramolecular Chemistry. *Acc. Chem. Res.* **1997**, *30*, 393–401. [CrossRef]

46. Elemans, J.A.A.W.; Rowan, A.E.; Nolte, R.J.M. Mastering molecular matter. Supramolecular architectures by hierarchical self-assembly. *J. Mater. Chem.* **2003**, *13*, 2661–2670. [CrossRef]

47. Yu, G.C.; Chen, X.Y. Host-Guest Chemistry in Supramolecular Theranostics. *Theranostics* **2019**, *9*, 3041–3074. [CrossRef] [PubMed]

48. Bickerton, L.E.; Johnson, T.G.; Kerckhoffs, A.; Langton, M.J. Supramolecular chemistry in lipid bilayer membranes. *Chem. Sci.* **2021**, *12*, 11252–11274. [CrossRef] [PubMed]

49. Kwon, T.; Choi, J.W.; Coskun, A. Prospect for Supramolecular Chemistry in High-Energy-Density Rechargeable Batteries. *Joule* **2019**, *3*, 662–682. [CrossRef]

50. Zhou, H.Y.; Yamada, T.; Kimizuka, N. Supramolecular Thermocells based on Thermo-Responsiveness of Host–Guest Chemistry. *Bull. Chem. Soc. Jpn.* **2021**, *94*, 1525–1546. [CrossRef]

51. Savyasachi, A.J.; Kotova, O.; Shanmugaraju, S.; Bradberry, S.J.; Ó'Máille, G.M.; Gunnlaugsson, T. Supramolecular Chemistry: A Toolkit for Soft Functional Materials and Organic Particles. *Chem* **2017**, *3*, 764–811. [CrossRef]

52. Düren, T.; Sarkisov, L.; Yaghi, O.M.; Snurr, R.Q. Design of new materials for methane storage. *Langmuir* **2005**, *20*, 2683–2689. [CrossRef] [PubMed]

53. Fukuhara, G. Analytical supramolecular chemistry: Colorimetric and fluorimetric chemosensors. *J. Photochem. Photobiol. C* **2020**, *42*, 100340. [CrossRef]

54. Zhang, L.-Y.; Zhao, X.-Y.; Wang, C.-M.; Yu, K.; Lv, J.-H.; Wang, C.-X.; Zhou, B.-B. The supercapacitor and photocatalytic supermolecule materials constructed by 4′4-pyridine and {$PMo_{12}O_{40}$}. *J. Solid State Chem.* **2022**, *312*, 123235. [CrossRef]

55. Sabina, G.I.; Octavian, D.P.; Nicolae, G.; Madalina, T.; Simona, M.C.; Vasile, I.P.; Bogdan, C.; Elisabeth, E.J. Use of Photocatalytically Active Supramolecular Organic–Inorganic Magnetic Composites as Efficient Route to Remove β-Lactam Antibiotics from Water. *Catalysts* **2022**, *12*, 1044.

56. Zhou, X.H.; Chen, Y.Y.; Wang, P.Y.; Xu, C.Y.; Yan, Q.S. Fabrication of AgI/BiPO₄ n–n heterojunction photocatalyst for efficient degradation of organic pollutants. *J. Mater. Sci. Mater. Electron.* **2020**, *31*, 12638–12648. [CrossRef]

57. Lu, J.R.; Yue, M.T.; Cui, W.Q.; Sun, C.H.; Liu, L. Supramolecular photocatalyst of perylene bisimide decorated with α-Fe_2O_3: Efficient photo-Fenton degradation of organic pollutants. *Colloids Surf. A Physicochem. Eng. Asp.* **2022**, *655*, 130222. [CrossRef]

58. Bao, S.H.; Wu, S.S.; Huang, L.P.; Xu, X.; Xu, R.; Li, Y.G.; Liang, Y.R.; Yang, M.Y.; Yoon, D.K.; Lee, M.; et al. Supramolecular Nanopumps with Chiral Recognition for Moving Organic Pollutants from Water. *ACS Appl. Mater. Interfaces* **2019**, *11*, 31220–31226. [CrossRef]

59. Wang, H.Y.; Hou, L.L.; Li, C.; Zhang, D.D.; Ma, P.T.; Wang, J.P.; Niu, J.Y. Synthesis, structure, and photocatalytic hydrogen evolution of a trimeric Nb/W addendum cluster. *RSC Adv.* **2017**, *7*, 36416–36420. [CrossRef]

60. Cao, P.Y.; Zhang, Y.P.; Gao, D.; Chen, H.X.; Zhou, M.L.; He, Y.F.; Song, P.F.; Wang, R.M. Constructing nano-heterojunction of MOFs with crystal regrowth for efficient degradation of tetracycline under visible light. *J. Alloys Compd.* **2022**, *904*, 164061. [CrossRef]

61. Abd El-Monaem, E.M.; Omer, A.M.; Khalifa, R.E.; Eltaweil, A.S. Floatable cellulose acetate beads embedded with flower-like zwitterionic binary MOF/PDA for efficient removal of tetracycline. *J. Colloid Interface Sci.* **2022**, *620*, 333–345. [CrossRef] [PubMed]

62. Zhang, Y.; Duoerkun, G.; Shi, Z.; Cao, W.; Liu, T.; Liu, J.; Zhang, L.; Li, M.; Chen, Z. Construction of TiO_2/Ag_3PO_4 nanojunctions on carbon fiber cloth for photocatalytically removing various organic pollutants in static or flowing wastewater. *J. Colloid Interface Sci.* **2020**, *571*, 213–221. [CrossRef] [PubMed]

63. Wu, F.; Zhou, F.; Zhu, Z.; Zhan, S.; He, Q. Enhanced photocatalytic activities of Ag_3PO_4/GO in tetracycline degradation. *Chem. Phys. Lett.* **2019**, *724*, 90–95. [CrossRef]

64. Eslami, A.; Bahrami, H.; Asadi, A.; Alinejad, A. Enhanced sonochemical degradation of tetracycline by sulfate radicals. *Water Sci. Technol.* **2016**, *287*, 131981. [CrossRef]

65. Hu, L.X.; Ren, X.H.; Yang, M.; Guo, W.L. Facet-controlled activation of persulfate by magnetite nanoparticles for the degradation of tetracycline. *Sep. Purif. Technol.* **2020**, *258*, 118014. [CrossRef]

66. Wu, X.F.; Wang, Y.J.; Song, L.J.; Su, J.Z.; Zhang, J.R.; Jia, Y.N.; Shang, J.L.; Nian, X.W.; Zhang, C.Y.; Sun, X.G. A yolk–shell Bi@void@SnO_2 photocatalyst with enhanced tetracycline degradation. *J. Mater. Sci. Mater. Electron.* **2019**, *30*, 14987–14994. [CrossRef]

67. Vladimir, A.; Anna, A.; Vadim, B.; Svetlana, K.; Varvara, V.; Daniil, K.; Madina, S.; Alexander, B.; Igor, F.; Roman, N.; et al. Fast Degradation of Tetracycline and Ciprofloxacin in Municipal Water under Hydrodynamic Cavitation/Plasma with CeO_2 Nanocatalyst. *Processes* **2022**, *10*, 2063.

68. Du, H.J.; Zhang, W.L.; Wang, C.H.; Niu, Y.Y.; Hou, H.W. A new nanocrystalline inorganic–organic hybrid exhibiting semiconducting properties and applications†. *Dalton Trans.* **2015**, *45*, 2624–2628. [CrossRef]
69. Beatríz, G.-A.; Ramón, M.-M.; José, V.R.-L.; Félix, S.; Juan, S. Discrimination between ω-amino acids with chromogenic acyclic tripodal receptors functionalized with stilbazolium dyes. *Tetrahedron Lett.* **2008**, *49*, 1997–2001.